ARTICLE

Room-Temperature Electric-Field Controlled Ferromagnetism in $Mn_{0.05}Ge_{0.95}$ Quantum Dots

Faxian Xiu,[†,*] Yong Wang,[‡] Jiyoung Kim,[†] Pramey Upadhyaya,[†] Yi Zhou,[†] Xufeng Kou,[†] Wei Han,[§] R. K. Kawakami,[§] Jin Zou,[‡] and Kang L. Wang[†]

[†]Device Research Laboratory, Department of Electrical Engineering, University of California, Los Angeles, California, 90095, [‡]Materials Engineering and Centre for Microscopy and Microanalysis, The University of Queensland, QLD 4072, Australia, and [§]Department of Physics, University of California, Riverside, California, 92521

ABSTRACT Room-temperature control of ferromagnetism by electric fields in magnetic semiconductors has been actively pursued as one of important approaches to realize practical spintronic and nonvolatile logic devices. While Mn-doped III−V semiconductors were considered as potential candidates for achieving this controllability, the search for an ideal material with high Curie temperature ($T_c > 300$ K) and controllable ferromagnetism at room temperature has continued for nearly a decade. Recently, $Mn_{0.05}Ge_{0.95}$ quantum dots (QDs) were demonstrated to have a T_c above 300 K. However, the field control of ferromagnetism based on hole-mediated effect remained at low temperatures and thus prohibited spintronic devices operable at ambient environment. Here, we report a successful demonstration of electric-field control of ferromagnetism in the $Mn_{0.05}Ge_{0.95}$ quantum dots up to 300 K. We show that, by using quantum structure, high-quality material can be obtained and effective hole mediation due to quantum confinement effect can be achieved. Upon the application of gate bias to a metal-oxide-semiconductor (MOS) capacitor, the ferromagnetism of the channel layer, that is, the $Mn_{0.05}Ge_{0.95}$ quantum dots, was manipulated through the change of hole concentration. Our results are fundamentally and technologically important toward the realization of room-temperature spin field-effect transistors and nonvolatile spin logic devices.

KEYWORDS: diluted magnetic semiconductors · spintronics · nonvolatile · $Mn_{0.05}Ge_{0.95}$ · quantum dots · electric-field controlled ferromagnetism · magnetic polarons

Electric field control of ferromagnetism has a potential to realize spin field-effect transistors (spin FETs) and nonvolatile spin logic devices *via* carrier-mediated effect.[1,2] With the manipulation of carrier spins, a new generation of nonvolatile (green) computing systems could be eventually developed for many low-power-dissipation applications in all fields, including sensor network, health monitoring, information, sustainable wireless system, *etc.* Since Datta and Das[3] first introduced the concept of spin FETs in 1990, enormous efforts were dedicated to creating a device wherein the carrier transport is modulated by electrostatic control of carrier spins.[4−12] One of the major challenges, however, is to find an ideal material with room-temperature controllable spin states.[4−7] In recent years, emerging dilute magnetic semiconductors (DMSs) became one of the promising candidates since they could possibly offer high T_c in excess of 300 K.[8] The demonstration of the carrier-mediated ferromagnetism involving correlated electron/hole systems leads to a para- to ferro-magnetism phase transition.[2,8−10] In principle, the collective alignment of spin states in these DMSs can be manipulated by the modulation of carrier concentrations through gate biasing in a FET structure.[6,11] For this kind of spin FETs, the "source" and "drain" may be completed through "nanomagnets", which are in turn controlled by the gate; and no carrier transport is needed. Clearly, one may also involve the control of source−drain conductance by gate-voltage-induced precession of injected spins (from the source). Since the early 2000s, significant progress on electric-field controlled ferromagnetism was achieved,[2,11−13] in which the ferromagnetism of a (In, Mn)As channel layer could be effectively turned on and off *via* electric fields in a gated FET. Such extraordinary field-modulated ferromagnetism immediately rendered the development of future spintronic devices. However, the manipulation of ferromagnetism was limited because of low T_c of the Mn-doped III−V materials.[14] Therefore, a search for new DMS materials with $T_c > 300$ K and carrier-mediated ferromagnetism becomes a current global challenge.[6,15]

Here we report a major breakthrough toward such room-temperature spin FETs and spin logic devices: a successful demonstration of electric-field controlled ferromagnetism up to 300 K. In our recent study, high T_c Mn-doped Ge QDs were achieved.[16] Their magnetic field-dependent magnetizations indicated a strong ferromagnetism above

*Address correspondence to xiu@ee.ucla.edu.

Received for review July 4, 2010 and accepted July 22, 2010.

Published online July 28, 2010. 10.1021/nn101516t

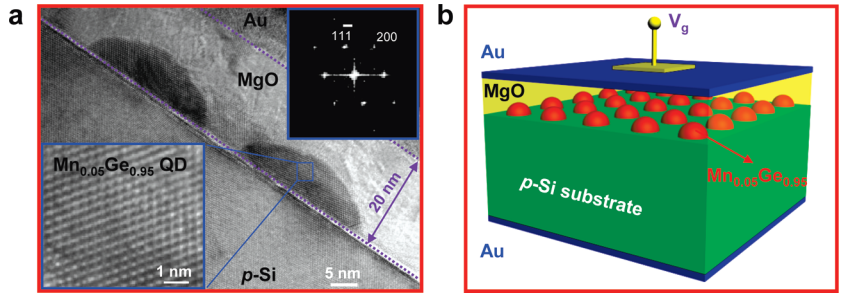

Figure 1. Structure of $Mn_{0.05}Ge_{0.95}$ MOS capacitor *via* TEM. (a) Cross-section high resolution TEM images of the $Mn_{0.05}Ge_{0.95}$ QDs grown on a *p*-Si substrate. Insets show an enlarged TEM picture and a diffraction pattern for an individual $Mn_{0.05}Ge_{0.95}$ QD, in which single crystallinity can be confirmed. The thickness of the gate dielectric (MgO) was estimated to be about 20 nm. The high resolution TEM reveals a polycrystalline MgO layer. (b) A schematic drawing of a MOS capacitor, consisting of electrodes (Au), MgO, $Mn_{0.05}Ge_{0.95}$ QDs, and *p*-type Si substrate. Note that there is a thin Mn_xGe_{1-x} wetting layer on top of Si. The wetting layer has a typical thickness of several angstroms. During SQUID measurements, the top electrode was biased while the bottom one was grounded.

400 K ($T_c > 400$ K). Magnetic force microscopy (MFM) measurements revealed a formation of a single magnetic domain in the $Mn_{0.05}Ge_{0.95}$ QDs and a switching behavior of dipole directions when the MFM tip magnetization polarity was reversed. The carrier-mediated ferromagnetism was identified with a MOS capacitor device, in which the electric-field controlled ferromagnetism was clearly observed by depleting holes out of the QD channel layer. In this study, we report the field-controlled ferromagnetism up to 300 K by using high-quality MgO as the gate dielectric grown by molecular beam epitaxy (MBE). We noted that the MBE-grown MgO layer significantly reduces the leakage current of the MOS capacitors in comparison with that of the Al_2O_3,[16] giving rise to much improved electric-field controllability on the ferromagnetism. The fact that the $Mn_{0.05}Ge_{0.95}$ QDs possess high Curie temperature[16] together with the room-temperature electric-field controlled ferromagnetism makes it technologically possible to fabricate practical spin devices, which can be operable at room temperature.

RESULTS AND DISCUSSION

Figure 1a shows a cross-section transmission electron microscopy (TEM) image of the MOS capacitor, consisting of electrodes (Au), MgO, $Mn_{0.05}Ge_{0.95}$ QDs, and *p*-type Si substrate. The $Mn_{0.05}Ge_{0.95}$ QDs have a dome shape with a base diameter of about 30 nm and a height of about 8 nm. The left-bottom inset is a high resolution TEM taken from a section of a QD, and it reveals the perfect crystalline lattice. A selective area electron diffraction pattern of the $Mn_{0.05}Ge_{0.95}$ QDs was also shown in the right-top inset, confirming that the Mn-doped Ge is a single-crystalline DMS. Extensive energy dispersive spectroscopy (EDS) and electron energy loss spectroscopy (EELS) studies revealed the presence of Mn (~5%) in the MnGe QDs; but importantly Mn aggregations were not detected within the resolution of the conventional TEM. No evident precipitates and phase separations of Mn_5Ge_3 and $Mn_{11}Ge_8$ were observed.[16] Figure 1b shows a schematic drawing of the MOS capacitor device structure. During the superconducting quantum interference device (SQUID) measurements, the top electrode was biased while the bottom one was grounded.

Figure 2 illustrates the electric-field controlled ferromagnetism performed at 100, 200, and 300 K, corresponding to panels a−c, d−f, and g−i, respectively. Due to the similarity of the data, we take the 100 K case as an example to describe the device operation (refer to Figure 2a−c). Figure 2 panels a and b show the hysteresis loops by SQUID with negative and positive biases on the MOS gate at 100 K, respectively. Under a negative bias, the holes are attracted into the channel of the device (accumulation mode). In this circumstance, however, the hysteresis loop does not show a noticeable change (Figure 2a). This can be explained by the fact that, even at zero volt, the QD device is already accumulated with enough holes to induce ferromagnetism; that is, the holes are sufficient to align the spins of a majority of the activated Mn ions in each individual dot. Further increasing negative bias does not change much on the hole concentration. On the contrary, with a positive bias, a large amount of holes are depleted into the *p*-type Si substrate, so that hole-mediated effect is notably reduced. The saturation moment per Mn ion decreases about 2.5 times as the gate bias increases from 0 to +40 V (Figure 2b). Figure 2c summarizes the change of remnant moments as a function of gate voltage. The inset in Figure 2c displays an enlarged picture to clearly show the variation of the remnant moments with respect to the gate bias. When the temperature was increased to 300 K (Figure 2g−i), the saturation and the remnant moments were modulated by ~23% and ~50% (at +40 V), respectively, which clearly showed the room-temperature controllable ferromagnetism, although it became less pronounced compared to those at 100 and 200 K (Figures 2c,f).

Device simulations using the MEDICI package[17] were performed to understand the distributions of holes in a QD. The simulated device structure was

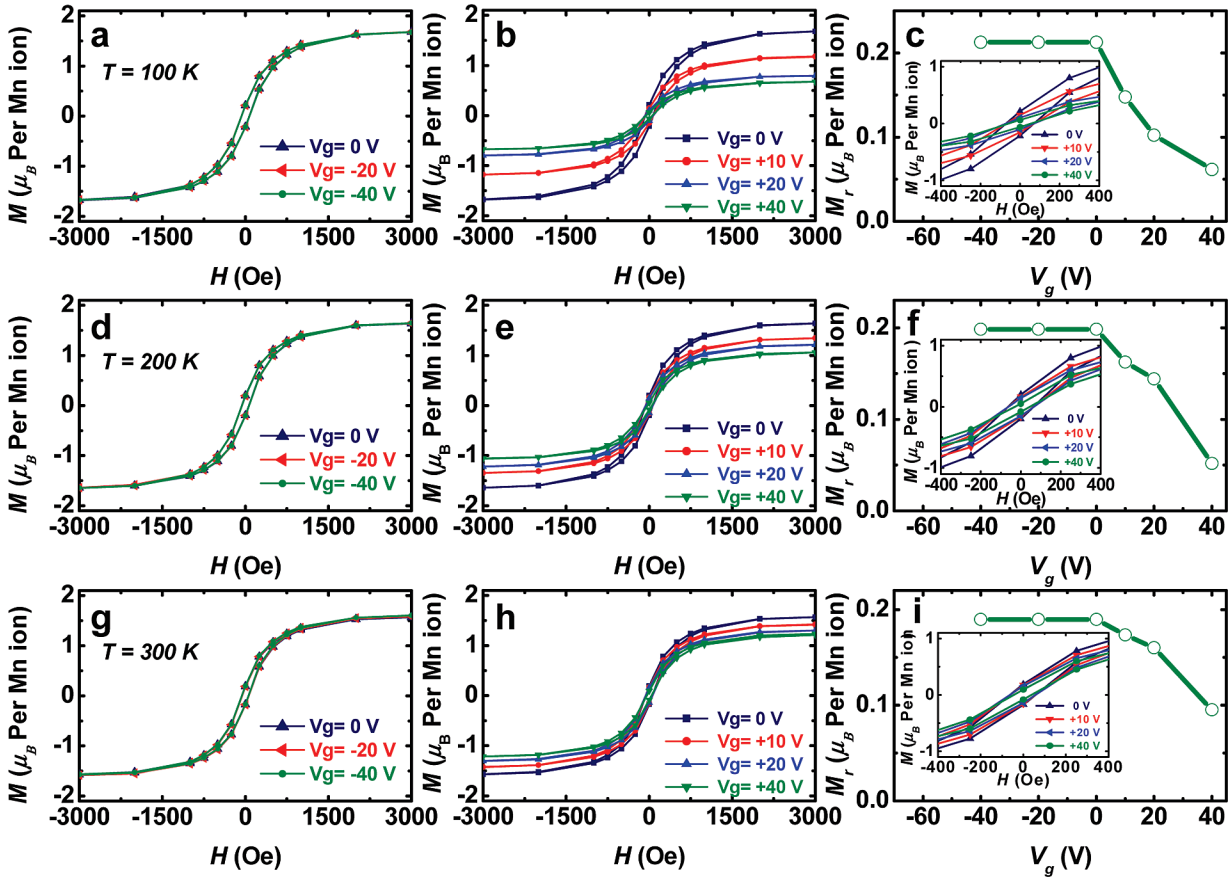

Figure 2. Control of ferromagnetism of $Mn_{0.05}Ge_{0.95}$ QDs by applying electric-field at 100 K (a−c), 200 K (d−f), and 300 K (g−i). Panels a, d, and g show the hysteresis loops with zero and negative bias of −10, −20, and −40 V on the gate. Panels b, e, and h show the hysteresis loops with zero and positive bias of +10, +20, and +40 V. Panels c, f, and I show remnant moments with respect to the gate bias. Insets of panels c, f, and I are enlarged figures from the central part of panels b, e, and h to clearly show the change of remnant moments, respectively. It is found that both the saturation and remnant moments can be manipulated by applying biases on the MOS gate. At low temperatures ($T < 200$ K), the manipulation of saturation moments is stronger compared with that of high temperatures ($T \geq 200$ K).

designed to fit the experimental conditions. The QDs were represented by a rectangle with a width of 50 nm, a height of 6 nm, and a spacing of 150 nm. Although Mn can have two acceptor levels in Ge,[18] during the simulation, only one shallower level (E_a = 0.16 eV) was considered because another deeper acceptor level (E_a = 0.37 eV) could barely contribute to the hole concentration. We also assumed that 60% of Mn atoms were activated in the modeling (according to the experimental data[16]). Since the simulations did not consider the formation of the impurity bands and the compensation effects that occur in the real experiments, the calculations may not give accurate hole concentrations. However, the fundamental physics of the field controlled ferromagnetism would not change since the capacitance−voltage measurements clearly revealed the carrier redistribution under the bias.[16] In the simulation, several physical models were adopted for accurate calculations, including the freeze-out effect at low temperature, the Fermi-Dirac model for carrier occupations, and quantum mechanical corrections by invoking the Philip's band gap widening effect.[17]

Figure 3 panels a−c show the calculated hole concentrations as a function of the gate voltage at 100, 200, and 300 K, respectively. At zero bias, due to the quantum confinement between the $Mn_{0.05}Ge_{0.95}$ QDs and *p*-type Si,[19] the hole concentration reaches 1.22×10^{18} and 2.08×10^{18} cm^{-3} for the top and center of the $Mn_{0.05}Ge_{0.95}$ QD, respectively (Figure 3a, 100 K). By applying a negative bias, holes start to accumulate in the $Mn_{0.05}Ge_{0.95}$ QD, leading to an increased hole concentration. For instance, at −10 V, the hole concentration increases eight times (1.65×10^{19} cm^{-3}) in the center of the dot, as calculated from Figure 3a. However, by applying a positive voltage, the holes are depleted into the *p*-type Si substrate. The hole concentration changes dramatically on the top surface of the $Mn_{0.05}Ge_{0.95}$ QDs ($\sim 10^{10}$ cm^{-3}), while, at the center region, the concentration of $10^{14}-10^{15}$ cm^{-3} remains in the voltage range of +2 to +10 V. Clearly, the top surface sensitively responds to the gate bias. Figure 3e illustrates the

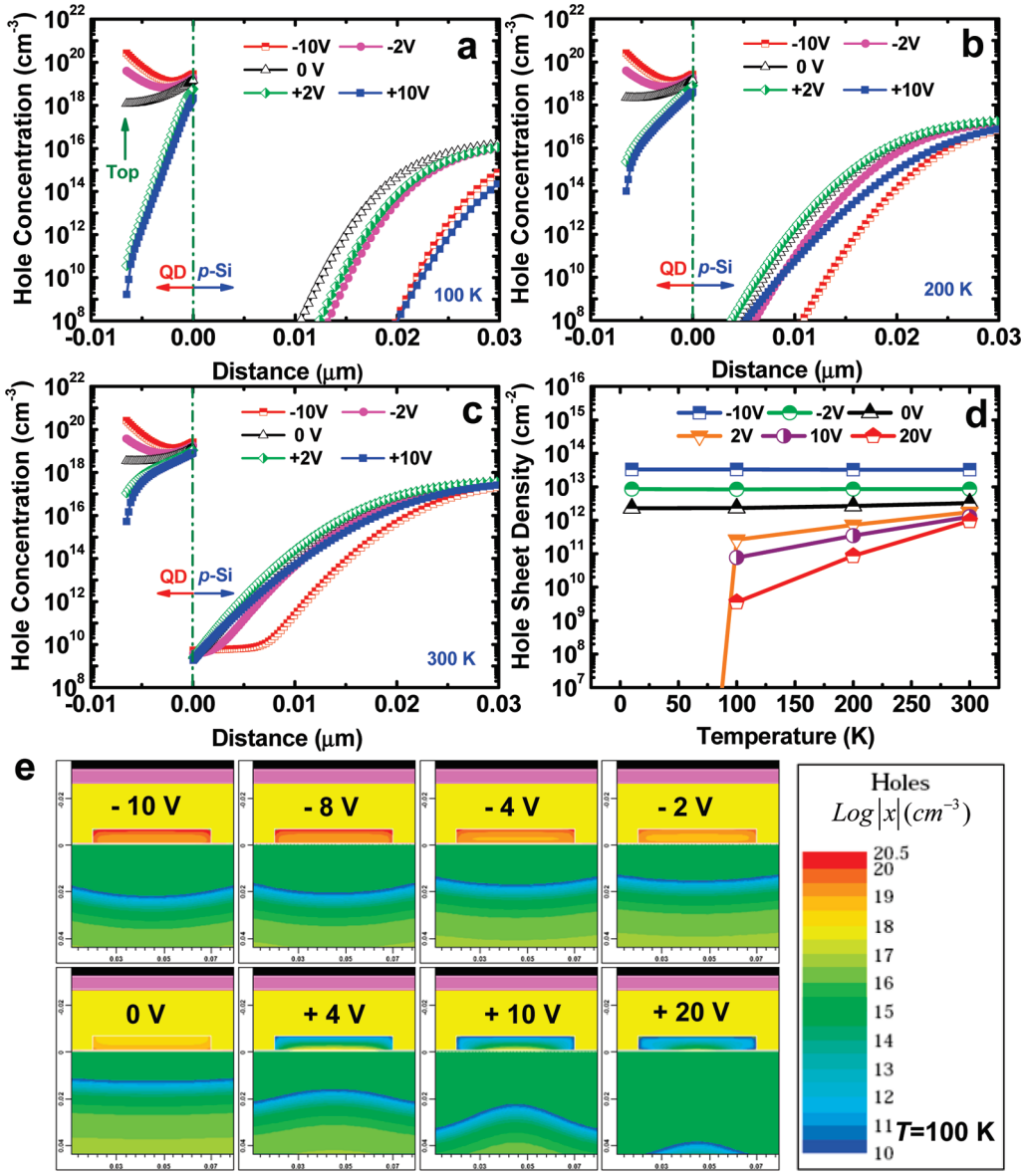

Figure 3. Simulated hole distributions for a MOS device using the $Mn_{0.05}Ge_{0.95}$ quantum dots as the channel layer: simulated hole concentrations at (a) 100, (b) 200, and (c) 300 K. Due to the Mn acceptor freeze-out effect, the depletion of holes inside the $Mn_{0.05}Ge_{0.95}$ QDs is much more pronounced at 100 K compared with that of 300 K. (d) Integrated sheet densities of holes over the entire $Mn_{0.05}Ge_{0.95}$ QD using a curvilinear integral method in Medici. Both temperature and voltage dependences of hole density are shown. (e) An example of hole redistribution map under different gate voltages at 100 K. The MOS device clearly shows accumulation and depletion processes under negative and positive gate biases, respectively.

redistribution of holes in the QD with gate biases at 100 K. It is noted that the hole concentration in the $Mn_{0.05}Ge_{0.95}$ QD decreases as the bias increases from −10 to +20 V; this result further confirms the hole accumulation, depletion, and inversion processes. Similarly, we have performed the simulations at 200 and 300 K in Figure 3 panels b and c, respectively. At +10 V, the top of the QD exhibits a high concentration of 10^{16} cm^{-3} at 300 K in comparison with that of 100 K ($\sim 10^{10}$ cm^{-3}), possibly resulting from the greater activation of the Mn impurities and thus a higher doping level of Mn in the QD. On the basis of these simulation results, we can conclude that the depletion process at high temperatures is not as strong as those at low temperatures. This explains the reduced controllability of ferromagnetism when the temperature approaches 300 K. Since the hole concentration varies with position inside the $Mn_{0.05}Ge_{0.95}$ QD, it is necessary to integrate the entire area of the QD and obtain a sheet density as an "effective" hole density, as shown in Figure 3d. In the accumulation mode (under zero and negative gate biases), the hole concentration does not have a noticeable temperature dependence from 10 to 300 K. However, in the depletion mode (positive biases), the holes were significantly depleted out of the $Mn_{0.05}Ge_{0.95}$ QD when the temperature decreases to below 100 K, primarily due to the freeze-out effect of

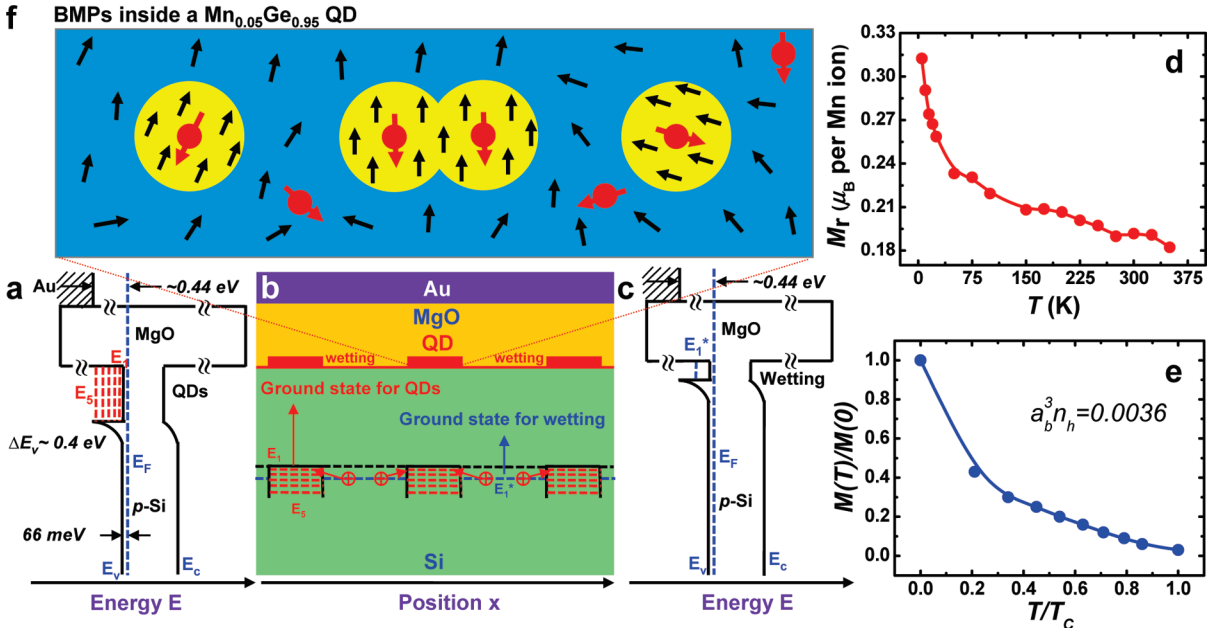

Figure 4. Energy band diagrams and a magnetic polaron model in the $Mn_{0.05}Ge_{0.95}$ QDs. (a, c) The energy band diagrams of MgO/$Mn_{0.05}Ge_{0.95}$ QD/Si and MgO/$Mn_{0.05}Ge_{0.95}$ wetting layer/Si, respectively. (b) A schematic drawing of the QDs and the wetting layer in real space. The energy band diagrams are also provided in the bottom to visualize the quantum confinement of the holes in the dots. (d) Remnant moments as a function of temperature at zero bias. A concave upward curve is observed. (e) Normalized remnant moments as a function of T/T_c. The concave nature is similar to that in panel d. (f) Formation of BMPs inside a single $Mn_{0.05}Ge_{0.95}$ QD. Small and large arrows show Mn impurity and hole spins, respectively. Some of BMPs are shown to overlap with each other to enhance ferromagnetism when a high density is developed (top panel).

the Mn acceptors.[18] Note that the electric-field controlled ferromagnetism is significantly improved compared with our earlier work,[10,16] which may be due to the optimized device structure and good quality MgO layer. The controllability could be dramatically affected by both the gate leakage and the activation process of Mn at different measurement temperatures.

Energy band diagrams of MgO/$Mn_{0.05}Ge_{0.95}$ QD/Si and MgO/$Mn_{0.05}Ge_{0.95}$ wetting layer/Si are schematically shown in Figure 4 panels a and c, respectively. By solving the Schrodinger equation for a rectangular quantum well with finite barriers,[20] we estimated that the $Mn_{0.05}Ge_{0.95}$ QDs have five quantized energy levels with $E_1 = 21$, $E_2 = 81$, $E_3 = 167$, $E_4 = 258$, and $E_5 = 331$ meV, as shown in Figure 4a. Among these levels, E_1 represents the ground state, that is, the lowest energy level. In contrast, the wetting layer exhibits a higher ground state of E_1* with a value of 142 meV. Since the energy of the ground state is much lower in the QDs, the majority of the holes would prefer to transfer into the dots, giving rise to a higher density of holes compared with that of the wetting layer. Figure 4b shows a schematic drawing of the QDs and the wetting layer in the real space. The energy band diagrams are also provided at the bottom of Figure 4b to visualize the transport of the holes. Note that due to the relatively large diameter of the $Mn_{0.05}Ge_{0.95}$ QDs (>30 nm), the quantum confinement in the horizontal direction is not significant compared with that in the vertical direction (perpendicular to the Si surface, or along the height of the QDs).

To explore the origin of the ferromagnetism in this material system, we plotted the measured remnant magnetizations as a function of temperature, $M(T)$ (Figure 4d), at zero bias, as the nature of $M(T)$ has been found crucial in understanding the underlying mechanism of DMS ferromagnetism.[21] The concave upward shape of $M(T)$ shown in Figure 4d is consistent with earlier reports of MnGe DMS,[9,22] which agrees well qualitatively with the percolation type of ferromagnetic transition. We also compare the dependence of calculated $M(T)$ (Figure 4e) using the percolation theory approach based on the magnetic polaron model proposed by Kaminski and Das Sarma,[23]

$$M(T)/M(0) = \beta[0.86 + (a_b{}^3 n_h)^{1/3} \ln(T_c/T)] \qquad (1)$$

where $M(0)$ *is the remnant moment at zero temperature;* β is the "infinite" cluster volume of overlapping spheres; a_b is the calculated Bohr radius[24] [a_b = 9.2 Å, Supporting Information]; and n_h is the hole concentration (4.7×10^{18} cm^{-3}, at zero bias, Figure 3d). It must be emphasized that given the minimal nature of the model one can only hope for a qualitative agreement and it is incorrect to try getting a quantitative agreement between theory and experiment by tuning the parameters of the above model.[21]

On the basis of above agreement on the shape of $M(T)$, we can construct a physical model based on the concept of bound magnetic polarons (BMPs) to explain

the observed field controlled ferromagnetism.[25] BMPs are regions of large magnetization resulting from all parallel polarized Mn spins. They are formed as a consequence of exchange interactions between the spins of localized carriers and magnetic ions, as illustrated in Figure 4f. Since the Mn doping concentration in our system is much larger than the hole concentration due in part to the compensation by Mn interstitials, BMPs could be developed with localized holes and a large number of Mn impurities around the hole localization center.[23] One can approximate several Mn ions to a sphere within a radius of r_h and assume that the Mn impurities contained inside this sphere interact with the hole and align their spins antiparallel to the hole spin, which results in the formation of a BMP.[26] The radius, r_h, grows with decreasing temperature given by $r_h \sim (a_b/2) \ln(J_0/k_BT)$,[27] where J_0 characterizes the strength of the exchange between carriers and magnetic ion. It was also shown that the nearby BMPs align ferromagnetically *via* effective coupling mediated by Mn spins lying in between the BMPs.[27,28] As a result, BMPs start to overlap and form percolated clusters aligned ferromagnetically as temperature decreases (Figure 4f).[23,26,28−31] From both theoretical calculations and experimental data, the MP formation was also found to be more favorable when the system dimension was reduced, particularly in the QDs case.[31−33] This phenomenon was explained by the fact that the quantum confinement could localize carriers in the proximity of magnetic ions and further strengthen the exchange interactions.[31−33] More interestingly, the binding energy of the MPs was remarkably enhanced when the system dimension is shrunk, resulting in a higher T_c in contrast to those of bulk materials.[31,34]

The above physical picture can be applied to explain the electric-field control of ferromagnetism in the $Mn_{0.05}Ge_{0.95}$ DMS system. The gate-controlled hole carriers in the $Mn_{0.05}Ge_{0.95}$ QDs may influence the formation of MPs and their interactions. If the holes density is sufficient, they can effectively mediate interactions between nearly all MPs in a dot.[35] When the hole density decreases in the depletion process, however, the amount of MPs can be reduced; and meanwhile, the overlapped MPs may start to uncouple and even disappear at low carrier densities, as illustrated in the outer MPs in Figure 4f, thus reducing the net magnetization moments. When the temperature increases toward room temperature, the MPs are subject to thermal fluctuation and become less stable compared to those at lower temperatures.[31,36] This is in agreement with the fact that the saturation moment decreases with increasing the temperature (zero bias). As mentioned earlier, the hole depletion process became less pronounced at 300 K when compared with that of low temperatures, for example, with +10 V, the holes on top of the QD do not change as much as those at 100 and 200 K (Figures 3a−c). This indicates that the QDs contain a large density of holes and possibly a high density of MPs at high temperatures because of more activation of the Mn acceptors, leading to a weak dependence of magnetization on the bias field. This analysis qualitatively explains the weak controllability of ferromagnetism at elevated temperatures. However, a detailed and quantitative theoretical treatise is still not available at this stage.

CONCLUSIONS

We demonstrated the field controlled ferromagnetism in the $Mn_{0.05}Ge_{0.95}$ QDs up to 300 K. The underlying physics lies in the effective hole-mediated ferromagnetism and improved material quality in quantum confined $Mn_{0.05}Ge_{0.95}$ dots. The variation of hole concentrations may directly affect the formation of the BMPs and their interactions, in turn controlling the magnetic moments of the $Mn_{0.05}Ge_{0.95}$ QDs. The obtained results shed light on the development of electric-field controlled spin logics and open up a new paradigm of nonvolatile systems for applications that may eventually resolve critical challenges of power dissipation and device miniaturization of today's microelectronics industry.

MATERIALS AND EXPERIMENTAL METHODS

The $Mn_{0.05}Ge_{0.95}$ QDs were grown on *p*-type Si substrates by a Perkin-Elmer solid-source MBE system. High-purity Ge (99.9999%) and Mn (99.99%) sources were evaporated by conventional high-temperature effusion cells. Prior to the growth, Si substrates were cleaned by a standard Radio Corporation of America method and thermal cleaning in the MBE chamber. The self-assembled $Mn_{0.05}Ge_{0.95}$ DMS quantum dots were subsequently deposited at 450 °C with a Ge growth rate of 0.2 Å/s and an adjustable Mn flux as the dopant source. The nominal thickness was designed to be 1.2 nm. The structural characteristics of the $Mn_{0.05}Ge_{0.95}$ QDs were investigated by TEM (a Philips F20 and a FEI Tecnai F30). The Mn composition and distribution were analyzed with EDS and EELS. For magnetic properties, a SQUID magnetometer from Quantum Design was utilized to measure field- and temperature-dependent magnetizations. As for device fabrications, MOS capacitors were made by depositing 20 nm-thick MgO on top of the $Mn_{0.05}Ge_{0.95}$ QDs layer *via* MBE (base pressure 1×10^{-10} Torr). The deposition of MgO layer is made by electron beam evaporation of a single crystal MgO source with a rate of ~1.0 Å/min measured by a quartz deposition monitor. Then the front and back sides were metalized with 200 nm-thick Au. After that, the MOS capacitors were loaded into the SQUID magnetometer to perform bias-dependent magnetization measurements at different temperatures.

Acknowledgment. We gratefully acknowledge the financial support from the Western Institute of Nanoelectronics (WIN), the Intel Spin-Gain FET project, and the Australian Research Council. We thank Dr. Jacob A. and Dr. Dmitri N. of Intel Incorporation for their advices on our experiments.

Supporting Information Available: More TEM images; Field controlled ferromagnetism at various temperatures; electrical properties of MOS devices; device simulations. This material is available free of charge *via* the Internet at http://pubs.acs.org.

REFERENCES AND NOTES

1. Awschalom, D. D.; Loss, D.; Samarth, N. *Semiconductor Spintronics and Quantum Computation*; Springer-Verlag: Berlin, Heidelberg, New York, 2002; pp 1−12.
2. Chiba, D.; Matsukura, F.; Ohno, H. Electrical Magnetization Reversal in Ferromagnetic III−V Semiconductors. *J. Appl. Phys. D* **2006**, *39*, R215–R225.
3. Datta, S.; Das, B. Electronic Analog of the Electro-optic Modulator. *Appl. Phys. Lett.* **1990**, *56*, 665–667.
4. Philip, J.; Punnoose, A.; Kim, B. I.; Reddy, K. M.; Layne, S.; Holmes, J. O.; Satpati, B.; LeClair, P. R.; Santos, T. S.; Moodera, J. S. Carrier-Controlled Ferromagnetism in Transparent Oxide Semiconductors. *Nat. Mater.* **2006**, *5*, 298–304.
5. Kanki, T.; Tanaka, H.; Kawai, T. Electric Control of Room Temperature Ferromagnetism in a $Pb(Zr_{0.2}Ti_{0.8})O_3/La_{0.85}Ba_{0.15}MnO_3$ Field-Effect Transistor. *Appl. Phys. Lett.* **2006**, *89*, 242506.
6. Dietl, T.; Ohno, H. Engineering Magnetism in Semiconductors. *Mater. Today* **2006**, *9*, 18–26.
7. Nepal, N.; Luen, M. O.; Zavada, J. M.; Bedair, S. M.; Frajtag, P.; El-Masry, N. A. electric-field Control of Room Temperature Ferromagnetism in III-N Dilute Magnetic Semiconductor Films. *Appl. Phys. Lett.* **2009**, *94*, 132505.
8. Dietl, T.; Ohno, H.; Matsukura, F.; Cibert, J.; Ferrand, D. Zener Model Description of Ferromagnetism in Zinc-Blende Magnetic Semiconductors. *Science* **2000**, *287*, 1019–1022.
9. Park, Y. D.; Hanbicki, A. T.; Erwin, S. C.; Hellberg, C. S.; Sullivan, J. M.; Mattson, J. E.; Ambrose, T. F.; Wilson, A.; Spanos, G.; Jonker, B. T. A Group-IV Ferromagnetic Semiconductor: Mn_xGe_{1-x}. *Science* **2002**, *295*, 651–654.
10. Chen, J.; Wang, K. L.; Galatsis, K. Electrical Field Control Magnetic Phase Transition in Nanostructured Mn_xGe_{1-x}. *Appl. Phys. Lett.* **2007**, *90*, 012501.
11. Ohno, H.; Chiba, D.; Matsukura, F.; Omiya, T.; Abe, E.; Dietl, T.; Ohno, Y.; Ohtani, K. Electric-Field Control of Ferromagnetism. *Nature* **2000**, *408*, 944–946.
12. Chiba, D.; Matsukura, F.; Ohno, H. Electric-Field Control of Ferromagnetism in (Ga, Mn)As. *Appl. Phys. Lett.* **2006**, *89*, 162505.
13. Chiba, D.; Sawicki, M.; Nishitani, Y.; Nakatani, Y.; Matsukura, F.; Ohno, H. Magnetization Vector Manipulation by Electric Fields. *Nature* **2008**, *455*, 515–518.
14. Weisheit, M.; Fahler, S.; Marty, A.; Souche, Y.; Poinsignon, C.; Givord, D. Electric Field-Induced Modification of Magnetism in Thin-Film Ferromagnets. *Science* **2007**, *315*, 349–351.
15. Jungwirth, T.; Sinova, J.; Masek, J.; Kucera, J.; MacDonald, A. H., III. Mn)V Semiconductors. *Rev. Mod. Phys.* **2006**, *78*, 809–864.
16. Xiu, F.; Wang, Y.; Kim, J.; Hong, A.; Tang, J.; Jacob, A. P.; Zou, J.; Wang, K. L. Electric-Field Controlled Ferromagnetism in High-Curie-Temperature $Mn_{0.05}Ge_{0.95}$ Quantum Dots. *Nat. Mater.* **2010**, *9*, 337–344.
17. *MEDICI, Two-Dimensional Semiconductor Device Simulation*; Technology Modeling Associates Inc.: Sunnyvale, CA, 2005.
18. Sze, S. *Physics of Semiconductor Devices*, 3rd ed.; Wiley:, New York, 2007; p 23.
19. Wang, K. L.; Thomas, S. G.; Tann, M. O. Sige Band Engineering for MOS, CMOS and Quantum Effect Devices. *J. Mater. Sci.-Mater. Electron.* **1995**, *6*, 311–324.
20. Schiff, L. I., *Quantum Mechanics*. 3rd ed.; McGraw-Hill: 1993; 1−50.
21. Das Sarma, S.; Hwang, E. H.; Kaminski, A. Temperature-Dependent Magnetization in Diluted Magnetic Semiconductors. *Phys. Rev. B* **2003**, *67*, 155201.
22. Li, A. P.; Shen, J.; Thompson, J. R.; Weitering, H. H. Ferromagnetic Percolation in Mn_xGe_{1-x} Dilute Magnetic Semiconductor. *Appl. Phys. Lett.* **2005**, *86*, 152507.
23. Kaminski, A.; Das Sarma, S. Polaron Percolation in Diluted Magnetic Semiconductors. *Phys. Rev. Lett.* **2002**, *88*, 247202.
24. Berciu, M.; Bhatt, R. N. Effects of Disorder on Ferromagnetism in Diluted Magnetic Semiconductors. *Phys. Rev. Lett.* **2001**, *87*, 107203.
25. Furdyna, J. K; Willardson, R. K; Beer, A. C. *Semiconductors and Semimetals*; Academic Press: New York, 1988; *Vol. 25*.
26. Sangaletti, L.; Canova, F. F.; Drera, G.; Salvinelli, G.; Mozzati, M. C.; Galinetto, P.; Speghini, A.; Bettinelli, M. Magnetic Polaron Percolation on a Rutile Lattice: A Geometrical Exploration in the Limit of Low Density of Magnetic Impurities. *Phys. Rev. B* **2009**, *80*, 033201.
27. Bhatt, R. N.; Berciu, M.; Kennett, M. P.; Wan, X. Diluted Magnetic Semiconductors in the Low Carrier Density Regime. *J. Supercond.* **2002**, *15*, 71–83.
28. Wolff, P. A.; Bhatt, R. N.; Durst, A. C. Polaron−Polaron Interactions in Diluted Magnetic Semiconductors. *J. Appl. Phys.* **1996**, *79*, 5196–5198.
29. Coey, J. M. D.; Venkatesan, M.; Fitzgerald, C. B. Donor Impurity Band Exchange in Dilute Ferromagnetic Oxides. *Nat. Mater.* **2005**, *4*, 173–179.
30. Durst, A. C.; Bhatt, R. N.; Wolff, P. A. Bound Magnetic Polaron Interactions in Insulating Doped Diluted Magnetic Semiconductors. *Phys. Rev. B* **2002**, *65*, 235205.
31. Bhattacharjee, A. K.; laGuillaume, C. B. A. Exciton Magnetic Polaron in Semimagnetic Semiconductor Nanocrystals. *Phys. Rev. B* **1997**, *55*, 10613–10620.
32. Yakovlev, D. R.; Uraltsev, I. N.; Ossau, W.; Landwehr, G.; Bicknell-Tassius, R. N.; Waag, A.; Schmeusser, S. Two-Dimensional Exciton Magnetic Polaron in Semimagnetic Quantum Wells. *Surf. Sci.* **1992**, *263*, 485–490.
33. Maksimov, A. A.; Bacher, G.; McDonald, A.; Kulakovskii, V. D.; Forchel, A.; Becker, C. R.; Landwehr, G.; Molenkamp, L. W. Magnetic Polarons in a Single Diluted Magnetic Semiconductor Quantum Dot. *Phys. Rev. B* **2000**, *62*, R7767–R7770.
34. Mackowski, S.; Gurung, T.; Nguyen, T. A.; Jackson, H. E.; Smith, L. M.; Kossut, J.; Karczewski, G. Optically Controlled Magnetization of Zero-Dimensional Magnetic Polarons in CdMnTe Self-Assembled Quantum Dots. *Phys. Status Solidi C* **2004**, 656–659.
35. MacDonald, A. H.; Schiffer, P.; Samarth, N. Ferromagnetic Semiconductors: Moving Beyond (Ga, Mn)As. *Nat. Mater.* **2005**, *4*, 195–202.
36. Stirner, T.; Hagston, W. E.; Harrison, P.; Goodwin, J. P. Exciton Magnetic Polarons in Quantum Wells. *J. Appl. Phys.* **1994**, *75*, 3466–3471.